

COMPUTATION OF CONJUGATE HEAT TRANSFER OVER A 2D CIRCULAR CYLINDER IN A LOW SPEED CROSSFLOW BY A GHOST CELL IMMERSSED BOUNDARY METHOD

Dartzi Pan

Department of Aeronautics and Astronautics,
National Cheng Kung University,
Tainan City, Taiwan, ROC
E-mail: dpan@mail.ncku.edu.tw

ABSTRACT

A ghost cell immersed boundary method is employed to compute the conjugate heat transfer over a circular cylinder in crossflow. The cylinder is internally heated by a circular surface of constant temperature. The conjugate heat transfer boundary treatment proposed at fluid-solid interface is shown to yield second order accurate solution. To demonstrate the capability of the current method, the location of the internal heating surface is varied to examine its effect on the heat transfer.

INTRODUCTION

Conjugate heat transfer is common in engineering problems involving internally heated solid components and external fluid flows. The conventional body-fitted grid method of solving conjugate heat transfer problems is to generate separate grids respectively for fluid domain and solid domain, to solve fluid flow equations and solid equations independently using different numerical methods, and to couple the two solutions together through boundary condition treatment at the fluid-solid interface. Recently immersed boundary method [1-5] has provided a way to solve both fluid and solid equations on one single Cartesian grid, greatly reducing the complexity involved when solving conjugate heat transfer problems. However, there are various types of immersed boundary method, each with its own merit or drawback. Hence, an immersed boundary method needs to be examined independently to identify its suitability to conjugate heat transfer problems.

On the fluid-solid interface, the no-slip boundary condition for velocity and the continuity of temperature distribution across the interface are Dirichlet type boundary condition. The conservation of heat conduction across the interface is Neumann type boundary condition. Thus, both kinds of boundary condition on the interface need to be treated accurately simultaneously when solving conjugate heat transfer problems. In this paper, a ghost cell immersed boundary method [6, 7, 8] capable of 2nd order accuracy for both Dirichlet and Neumann boundary condition is employed to solve conjugate heat transfer problems. A model conjugate heat transfer problem is used to verify the accuracy of the proposed boundary treatment. To demonstrate the capability of the developed method, an internally heated circular cylinder in a crossflow is computed. The location of the internal heating

surface is varied to examine its effects on the heat transfer over the cylinder.

GOVERNING EQUATIONS

The integral incompressible Navier-Stokes equations are

$$\oint_{CS} \bar{v} \cdot d\bar{S} = 0$$

$$\frac{\partial}{\partial t} \int_{CV} \bar{v} dV + \oint_{CS} \bar{v} \bar{v} \cdot d\bar{S} - \oint_{CS} \frac{1}{Re} \bar{\nabla} \bar{v} \cdot d\bar{S} + \int_{CV} \frac{\bar{G}r}{Re^2} \theta_f dV + \oint_{CS} P d\bar{S} = 0 \quad (1)$$

$$\frac{\partial}{\partial t} \int_{CV} \theta_f dV + \oint_{CS} \theta_f \bar{v} \cdot d\bar{S} - \oint_{CS} \frac{1}{Pr Re} \bar{\nabla} \theta_f \cdot d\bar{S} = 0$$

where \bar{v} is velocity, P is pressure, θ_f is fluid temperature with subscript f , Re is the free stream Reynolds number, Pr is the free stream Prandtl number, $\bar{G}r$ is the vector form Grashof number for gravitational forces, CS indicates Control Surface, CV indicates Control Volume. For the solid domain, the governing equations for heat conduction is

$$\frac{\partial}{\partial t} \int_{CV} \theta_s dV - \oint_{CS} \left(\frac{\alpha_s}{\alpha_f} \frac{1}{Pr Re} \right) \bar{\nabla} \theta_s \cdot d\bar{S} = 0 \quad (2)$$

where θ_s is the solid temperature with subscript s , α_s is the solid thermal diffusivity, α_f is the fluid thermal diffusivity. In steady state, Eq. (2) is a Laplace equation. All variables in Eq. (1) and (2) are properly non-dimensionalized by respective reference values. In particular, temperature is normalized as $\theta = \frac{T - T_\infty}{T_{ref} - T_\infty}$, where T_∞ is the free stream temperature, T_{ref} is a given reference temperature, here it is the temperature of the heating surface.

On the fluid-solid interface, the no-slip boundary condition for velocity is applied. For temperature, the boundary conditions at the interface are

$$\theta_f = \theta_s$$

$$k_f \frac{\partial \theta_f}{\partial n} = k_s \frac{\partial \theta_s}{\partial n} \quad (3)$$

where k_f is the fluid thermal conductivity, and n is the distance along interface normal. The first equation of Eq. (3) enforces the continuity of temperature distribution and the second equation indicates the conservation of conduction heat across the interface.

FINITE VOLUME METHOD

One single Cartesian grid is generated to cover both fluid and solid domains. The same cell-centered finite volume discretization method [6,7,8] is applied to both fluid and solid equations. For flow computations, Eq. (1) is solved by an implicit pressure correction method. Keeping the pressure fixed at the current time and using implicit time integration, the fully discretized finite volume equation is

$$\left(\frac{c_1 Q^* - c_2 Q^n + c_3 Q^{n-1}}{\Delta t} + R_{conv}^* - R_{vis}^* - H^* + R_P^n + F_{dir} \right) \Delta V = 0 \quad (4)$$

where the superscript “*” represents the intermediate state, “n” indicates the current time level; ΔV is the volume of the considered cell; Δt is the time increment; $Q = [u \ v \ \theta]^T$ is the vector of conserved variables per unit volume; R_{conv} , R_P and R_{vis} are the vector of surface integral of convective, pressure and viscous fluxes respectively over the control surface CS divided by ΔV ; H is vector of the source terms per unit volume; F_{dir} is a direct forcing per unit volume added to forcing points in order to model the presence of immersed bodies. The constants are $c_1=1.5$, $c_2=2$ and $c_3=0.5$ for the second-order backward differencing scheme, and $c_1=1$, $c_2=1$ and $c_3=0$ for the first-order Euler implicit scheme. The intermediate velocity \bar{v}^* generally does not satisfy the divergence-free condition. The velocity and the pressure are corrected as

$$\begin{aligned} \bar{v}^{n+1} &= \bar{v}^* - \Delta t \bar{\nabla} \phi^n \\ P^{n+1} &= P^n + \phi^n \end{aligned} \quad (5)$$

By requiring \bar{v}^{n+1} be divergence-free, we obtain the Poisson equation:

$$\nabla^2 \phi^n - \frac{\bar{\nabla} \cdot \bar{v}^*}{\Delta t} = 0 \quad (6)$$

which is to be solved for the pressure correction ϕ^n . For steady-state computations, the time integration is continued by taking $\theta^{n+1} = \theta^*$ after Eq. (4) to Eq. (6).

As for the solid temperature computations on the solid domain, the same discretization and time marching method as those for fluid temperature are used. During each time marching step, Eq. (1) and Eq. (2) are solved in sequence and multigrid sub-iterations are used to drive the time accurate fluid and solid equations to their convergence independently.

A GHOST CELL IMMERSSED BOUNDARY METHOD

The ghost cell system is defined for fluid domain and solid domain separately and independently. For flow computations, the ghost cells (in solid domain), their projection points (on interface) and their image points (in fluid domain) are depicted in Fig. 1. Here the empty squares are the fluid cell centers whose values are to be solved, the triangles are the ghost cell centers whose values are to be assigned in order to implicitly enforce appropriate boundary conditions at their projection points respectively, and the filled squares are the solid cells which play no role in flow computations. The ghost cells for flow computation are the first layer of cells on the solid side

adjacent to the fluid-body interface with at least one neighboring fluid cell. Along their projection lines onto the interface, the image points are a distance δ into the fluid domain, as shown in Fig. 1. Here $\delta = \sqrt{2}\Delta x$ is taken in 2D to ensure that the image points are surrounded by fluid cell centers not involving any ghost centers.

For solid computations, a similar set of ghost cells (in fluid domain), their projection points (on interface) and their image points (in solid domain) will be defined separately and independently. In this case the ghost cells are the first layer of cells on the fluid side adjacent to the interface with at least one neighboring solid cell. The image points are located a distance δ from the interface into the solid domain.

The values at ghost cell centers are obtained by extrapolation from the solution domain. Their values are designed to implicitly enforce the required boundary conditions at their projection points on the interface. A general representation of the boundary condition at a projection point can be expressed by

$$s \left(\frac{\partial Q}{\partial n_w} \right)_{proj} + t Q_{proj} = q \quad (7)$$

where n_w indicates the outward surface normal pointing into the solution domain (fluid domain in this example), $\left(\frac{\partial Q}{\partial n_w} \right)_{proj}$

is the normal variable gradient at the projection point, Q_{proj} is the variable value at the projection point, q is the boundary value given at the projection point; the coefficients s and t determine the type of the boundary condition. It is clear that the constant set ($s=0$, $t=1$) indicates Dirichlet condition, ($s=1$, $t=0$) indicates Neumann condition, and ($s=1$, $t=1$) indicates Robin condition. The ghost-cell direct forcing approach is simply an appropriate solution reconstruction procedure to set the ghost cell values such that Eq. (7) is satisfied implicitly on the immersed boundary.

The variable value Q_{image} can be obtained easily by a bilinear interpolation utilizing the variable values of the four fluid centers enclosing the image point. A bi-linear approximation for $\left(\frac{\partial Q}{\partial n_w} \right)_{image}$ can also be done easily with known direction vector \hat{n}_w . A 2-point second-order polynomial reconstruction along n_w can be obtained by solving

$$\begin{bmatrix} 2\delta & 1 & 0 \\ \delta^2 & \delta & 1 \\ 0 & s & t \end{bmatrix} \begin{bmatrix} a_2 \\ a_1 \\ a_0 \end{bmatrix} = \begin{bmatrix} \left(\frac{\partial Q}{\partial n_w} \right)_{image} \\ Q_{image} \\ q \end{bmatrix} \quad (8)$$

for the coefficient a_2 , a_1 and a_0 . For a target point on the surface normal passing through the projection point, its variable value Q_{target} can be interpolated or extrapolated by

$$Q_{target} = a_2 r_n^2 + a_1 r_n + a_0 \quad (9)$$

where r_n is the outward normal distance between the target point and the projection point. The ghost value Q_{ghost} can be

extrapolated by taking $r_n = -|\vec{r}_{ghost} - \vec{r}_{proj}|$ in Eq. (9), where \vec{r}_{ghost} and \vec{r}_{proj} are the position vector of the ghost center and the projection point, respectively. Note that here r_n is negative and Q_{ghost} is obtained by an extrapolation. It has been shown [6, 7, 8] that Eq. (8) and Eq. (9) yield 2nd-order accurate solution in L2 sense for both Dirichlet and Neumann boundary conditions.

FLUID-SOLID CONJUGATE HEAT TRANSFER

In theory, the two boundary conditions in Eq. (3) need be satisfied simultaneously. In practice, since the flow domain and the solid domain are solved in sequence during one time step, the two equations in Eq. (3) are also enforced in sequence. When $k_s > k_f$, it is chosen to enforce for solid computation that

$$\frac{\partial \theta_s}{\partial n} = \left(\frac{k_f}{k_s}\right) \frac{\partial \theta_f}{\partial n} \quad (10)$$

That is, $\left(\frac{k_f}{k_s}\right) \frac{\partial \theta_f}{\partial n}$ at the interface is estimated by the flow

solution θ_f , then it is assigned to gradient $\frac{\partial \theta_s}{\partial n}$ at the interface via the Neumann boundary condition treatment for the solid temperature. Note that the condition $\frac{k_f}{k_s} < 1$ indicates

$\left|\frac{\partial \theta_s}{\partial n}\right| < \left|\frac{\partial \theta_f}{\partial n}\right|$, which gives a better stability when enforcing

Neumann boundary condition in the solid computation.

The other boundary condition is enforced in fluid computation, that is,

$$\theta_f = \theta_s \quad (11)$$

The interface temperature is estimated using the solid temperature θ_s at the interface, and then it is assigned to θ_f at the interface via the Dirichlet boundary condition treatment for the fluid temperature.

In the case when $\frac{k_s}{k_f} < 1$, the Neumann boundary condition on the interface should be enforced in the flow computation, leaving the Dirichlet boundary condition to the solid computation.

VALIDATEION

The heat transfer problem of among three coaxial circular cylinders is depicted in Fig. 2, which is a copy from Ref. [1]. The inner cylinder has a radius $R_i = 0.45$, the middle cylinder has $R_m = 0.9$, and the outer cylinder has $R_o = 1.8$. The inner cylinder surface is fixed at a surface temperature $\theta_i = 1$. The annular space between R_i and R_m is filled with a solid, while the annular space between R_m and R_o is filled with a fluid. The outer cylinder surface at R_o is rotating at a circumferential

speed $U_o = 1$. It drives a rotational flow in the annular space between R_m and R_o . The surface temperature at R_o is fixed at $\theta_o = 0$. There is conjugate heat transfer across the middle cylinder surface. The analytical solution of this model problem can be found in Ref. [1].

Note that the steady state temperature distribution is solely determined by the heat conduction process. The rotational speed U_o has no effect on the steady state temperature distribution. Hence this problem is computed here on Cartesian grid of various sizes with $U_o = 0$. The computational domain is a square of length 4 covering the three cylinder surfaces. Figure 3 shows the temperature distribution along the horizontal line passing through cylinder center on a 64×64 grid for $k_s = 10k_f$, and Fig. 4 is for $k_s = 0.1k_f$. The symbols are computed results, which are in excellent agreement with the exact solutions. Using data computed along the horizontal grid line passing through cylinder center, Fig. 5 shows the convergence test using 64×64, 128×128 and 256×256 grids. The estimated order of accuracy is 1.94 in L2 norms for $k_s = 0.1k_f$ and 1.71 for $k_s = 10k_f$. This validates that the current ghost cell method is second order accurate when applied to conjugate heat transfer problems. Although not shown here, but if only a first-order estimation of temperature gradient at the projection points on the interface, then only first order accuracy is observed.

INTERNALLY HEATED CIRCULAR CYLINDER

The conjugate heat transfer characteristics of a cylinder with one or multiple layers of solid materials between the internal heating element and the external crossflow have important implications to crossflow heat exchangers [9]. In this paper, a computational model of internally heated cylinder is made of a cylinder of unit diameter with an internal circular surface of diameter 0.2 at fixed temperature $\theta = 1$. Heat is transported from the internal heating surface to the cylinder surface by pure conduction, and eventually is transported away from the cylinder surface by convection and conduction. The conductivity ratio is taken to be $k_s/k_f = 9$. The Reynolds number based on cylinder diameter, the free stream velocity and the fluid dynamic viscosity is $Re = 40$. The Prandtl number is set to 0.71. The Grashof number is zero. We are interested in steady state temperature distributions, where the solid equation is a Laplace equation.

The Cartesian grid has a total of 51720 cells covering a computational domain of size 60×60. The grid is locally refined such that there are about 68.3 cells along the cylinder diameter and about 13.6 cells along the internal surface diameter. The free stream condition is set to the inflow boundary and the two side boundaries. The free stream temperature is $\theta = 0$. The downstream boundary follows the upwind differenced equation of $(\partial Q / \partial t) + U_n (\partial Q / \partial x) = 0$, where U_n is the computed normal outflow velocity at the boundary. Since only the steady state solution is of interest, the implicit Euler method is used in time integration for fluid and

solid. The diffusivity ratio $\frac{\alpha_s}{\alpha_f}$ can be arbitrarily chosen to accelerate the convergence.

Figure 5 to Fig. 10 show the temperature contours inside and outside the cylinder with the heating surface center (x_c, y_c) located in different positions. With zero Grashof number, the temperature equation in Eq. (1) is decoupled from the momentum equations. Thus the velocity field computed for all cases show here are identical to the computer machine accuracy. The identical streamline patterns in Fig. 5 to Fig. 10 reflect this fact. Note that the temperature field is symmetric with respect to x axis in Fig. 5 to Fig. 7, and asymmetric in Fig. 8 to Fig. 10 due to the position of the heating surface. The discontinuous slope in temperature contours across the cylinder surface due to the jump in conductivity can be clearly seen in these figures.

To compute the heat transfer H_{Body} over the body surface, the following surface integrals are used:

$$H_{Body} = \sum_{surface} \frac{1}{Pr Re} \bar{\nabla} \theta_f \cdot \Delta \bar{S} \quad (12)$$

where the summation is performed on all boundary segments of the body surface. The temperature gradients are obtained by the bi-linear approximation described previously using the surrounding cell vertex values. Table 1 lists the computed heat transfer times the constant $RePr$ with varying heating surface locations. Note that heat transfer increases when heating surface moves toward the upstream stagnation (6th row to 2nd row). This is reasonable, because the heat convection starts from the upstream stagnation, and more heat will be convected downstream when the heat source is closer to the upstream stagnation.

CONCLUSIONS

This paper demonstrates the application of a ghost cell immersed boundary method in solving conjugate heat transfer problems. The same finite volume discretization method is used on one single Cartesian grid to solve the governing equations for both fluid and solid phases. This approach is advantageous when compared with the traditional approach that uses different discretization methods and different body-fitted grids for different phases. It is shown that the present treatment across the solid-fluid interface yields second-order accurate solution in L2 norm. The examples of a circular cylinder in a low speed crossflow with an internal heating surface located in various locations demonstrate the capability of the present method to treat complex geometry.

ACKNOWLEDGEMENTS

This work is funded by the Ministry of Science and Technology of Taiwan, ROC under project MOST104-2221-E-006-108. The support is highly appreciated.

REFERENCES

[1] De Tullio, M. D., Latorre, S. S., De Palma, P., Napolitano, M., Pascasio, G., An Immersed Boundary Method for

Solving Conjugate Heat Transfer Problems in Turbomachinery, Proceedings of ECCOMAS CFD 2010, Lisbon, Portugal, 14-17 June 2010.

- [2] Xie, W. and DesJardin, P. E., A Level Set Embedded Interface Method for Conjugate Heat Transfer Simulations of Low Speed 2D flows, *Computers & Fluids*, vol. 37, 2008, pp. 1262-1275.
- [3] Nagendra, K., Tafti, D. K. and Viswanath, K., A New Approach for Conjugate Heat Transfer problems Using Immersed Boundary Method for Curvilinear Grid-based Solvers, *Journal of Computational Physics*, vol. 267, 2014, pp. 225-246.
- [4] Hu, Y., Li, D., Shu, S., Niu, X., Simulation of Steady Fluid-solid Conjugate Heat Transfer Problems via Immersed Boundary-Lattice Boltzmann method, *Computers and Mathematics with Applications*, vol. 70, 2015, pp. 2227-2237.
- [5] Jeon, B. J., Kim, Y.S., and Choi, H.G., Effect of the Reynolds Number on the Conjugate Heat Transfer Around a Circular Cylinder with Heat Source, *Journal of Mechanical Science and Technology*, vol. 26, No. 12, 2012, pp. 3849-3855.
- [6] Pan, D., A Comparison of Fluid-cell and Ghost-cell Direct Forcing Immersed Boundary Method for Incompressible Flows with Heat Transfer", *Numerical Heat Transfer, Part B, Fundamentals*, Vol. 68, 2015, pp. 30-52.
- [7] Pan, D., A General Boundary Condition Treatment in Immersed Boundary Methods for Incompressible Navier-Stokes Equations with Heat Transfer, *Numerical Heat Transfer, Part B, Fundamentals*, Vol. 61, 2012, pp. 279-297.
- [8] Pan, D., A Simple and Accurate Ghost Cell Method for the Computation of Incompressible Flows over Immersed Bodies with Heat Transfer, *Numerical Heat Transfer, Part B, Fundamentals*, Vol. 58, 2010, pp. 17-39.
- [9] Kaptan, K., Buyruk, E., and Ecder, A., Numerical Investigation of Fouling on Cross-flow Heat Exchanger Tubes with Conjugated Heat Transfer Approach, *International Communications in Heat and Mass Transfer*, vol. 35, 2008, pp. 1153-1158.

Table 1 Heat transfer over cylinder surface with internal heating surface at various positions, $Re=40$, $Ks/Kf=9$

Center (x_c, y_c)	$H_{Body} Re Pr$
(-0.25, 0)	8.0301
(-0.177, 0.177)	7.9942
(0, 0.25)	7.8012
(0.177, 0.177)	7.5220
(0.25, 0)	7.3903
(0, 0)	7.9424

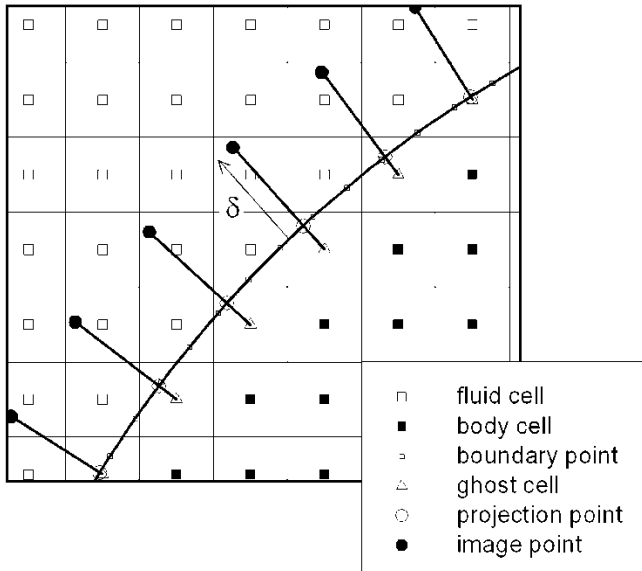


Figure 1 Depict of fluid flow domain and its ghost cell system.

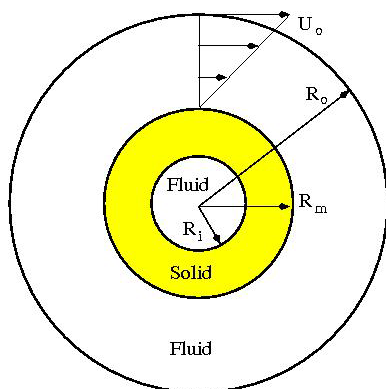


Figure 2 Depict of heat transfer problem for the solid and the rotational flow in annular spaces. (Copy from Ref. [1])

Temperature Along Horizontal Line $dx=1/16, Ks/Kf=10$

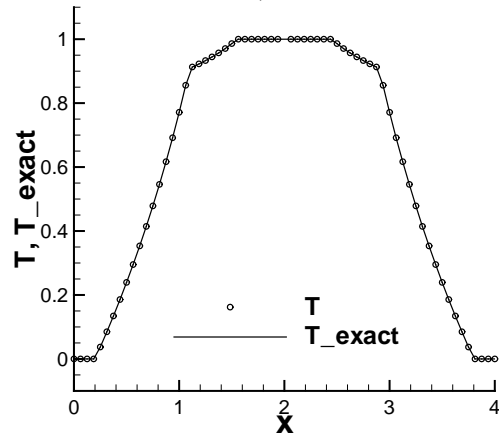


Figure 3 Temperature distribution along central horizontal grid line, center at $x=2$, $Ks/Kf=10$, symbols: computed, line: exact.

Temperature Along Horizontal Line $dx=1/16, Ks/Kf=0.1$

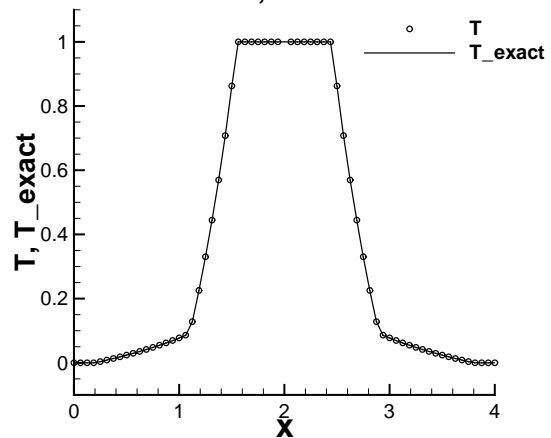


Figure 3 Temperature distribution along central horizontal grid line, center at $x=2$, $Ks/Kf=0.1$, symbols: computed, line: exact.

3-Cylinder Conjugate Heat Transfer

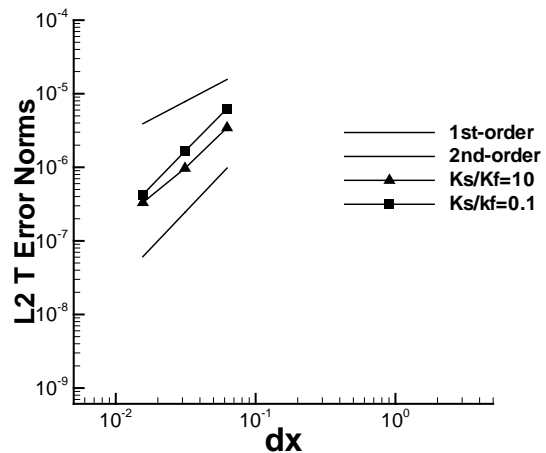


Figure 4 Order analysis using temperature along central horizontal grid line, Squares: $Ks/Kf=0.1$, triangles: $Ks/Kf=10$.

Temperature Contours and Streamlines
 $k_s/k_f=9$, $Re=40$, Center $(-0.25, 0)$

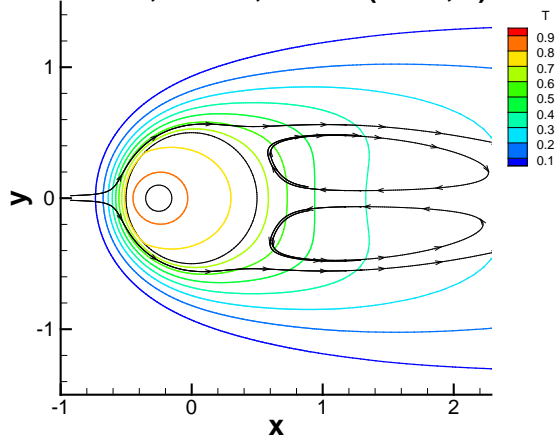


Figure 5 Temperature contours and streamlines, heating surface at $(-0.25, 0)$, $K_s/K_f=9$, $Re=40$

Temperature Contours and Streamlines
 $k_s/k_f=9$, $Re=40$, Center $(-0.177, 0.177)$

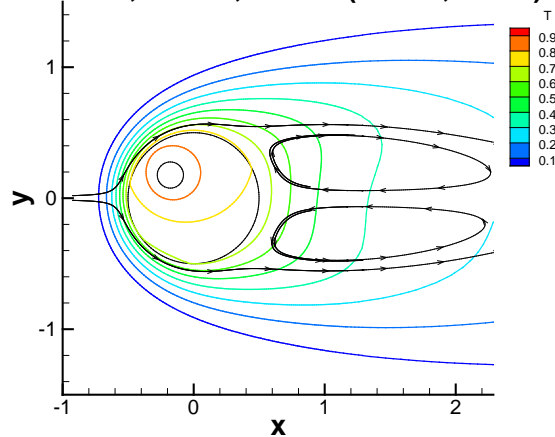


Figure 8 Temperature contours and streamlines, heating surface at $(-0.177, 0.177)$, $K_s/K_f=9$, $Re=40$

Temperature Contours and Streamlines
 $k_s/k_f=9$, $Re=40$, Center $(0, 0)$

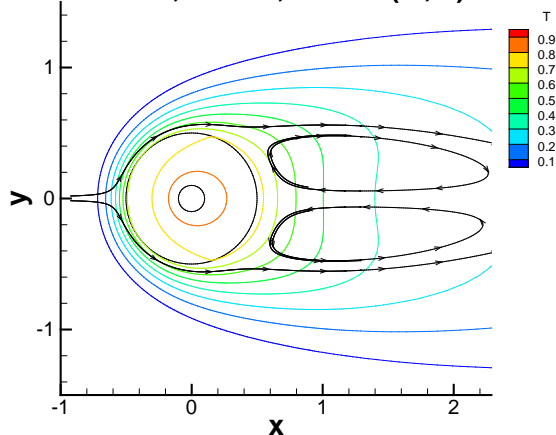


Figure 6 Temperature contours and streamlines, heating surface at $(0, 0)$, $K_s/K_f=9$, $Re=40$.

Temperature Contours and Streamlines
 $k_s/k_f=9$, $Re=40$, Center $(0, 0.25)$

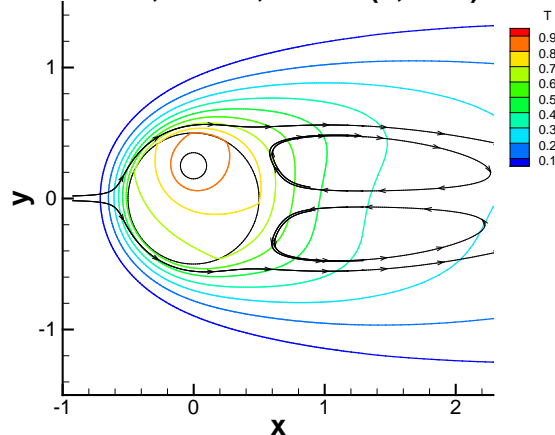


Figure 9 Temperature contours and streamlines, heating surface at $(0, 0.25)$, $K_s/K_f=9$, $Re=40$

Temperature Contours and Streamlines
 $k_s/k_f=9$, $Re=40$, Center $(0.25, 0)$

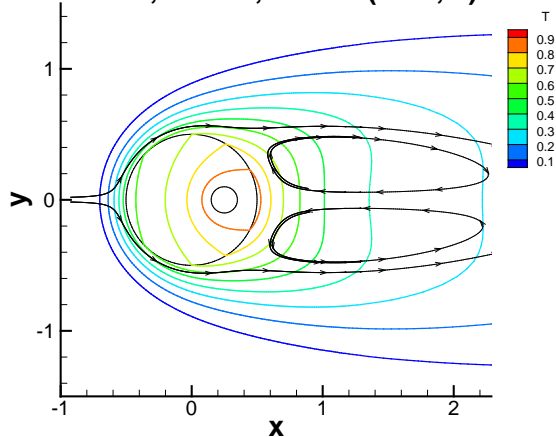


Figure 7 Temperature contours and streamlines, heating surface at $(0.25, 0)$, $K_s/K_f=9$, $Re=40$

Temperature Contours and Streamlines
 $k_s/k_f=9$, $Re=40$, Center $(0.177, 0.177)$

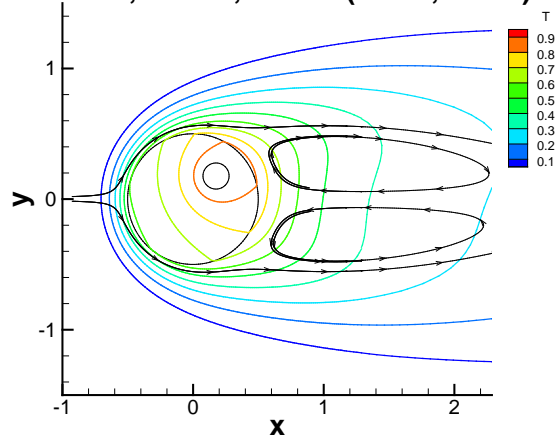


Figure 10 Temperature contours and streamlines, heating surface at $(0.177, 0.177)$, $K_s/K_f=9$, $Re=40$